Title

Anisotropic Growth of TiO2 onto Gold Nanorods for Plasmon-Enhanced Hydrogen Production from Water Reduction.

Journal

Journal of the American Chemical Society, 138(4)

ISSN

0002-7863

Authors

Wu, Binghui
Liu, Deyu
Mubeen, Syed
et al.

Publication Date

2016-02-01

DOI

10.1021/jacs.5b11341

Anisotropic Growth of TiO_2 onto Au Nanorods for Plasmon-Enhanced Hydrogen Production from Water Reduction

Binghui Wu,[†,‡,§] Deyu Liu,[†,§] Syed Mubeen,[†,#] Tracy T Chuong,[†] Martin Moskovits,[†] and Galen D. Stucky[†,‡,*]

[†]Department of Chemistry & Biochemistry, University of California, Santa Barbara, California 93106, USA

[‡]Collaborative Innovation Center of Chemistry for Energy Materials, Xiamen University, Xiamen 361005, China

ABSTRACT: Plasmonic-metal/semiconductor hetero-structures show promise as absorbers/catalysts for visible-light-driven photocatalysis. Au nanorods (AuNRs) semi-coated with TiO_2 are expected to be ideally structured systems for hydrogen evolution. Synthesizing such structures by wet-chemistry methods, however, has proved challenging. Here we report the bottom-up synthesis of AuNR-TiO_2 nanodumbbells with spatially separated gold/TiO_2 regions, whose structures are governed by the NRs' diameter, and the higher curvature and lower density of C_nTAB surfactant at the NRs' tips than on their lateral surfaces, as well as the morphology's dependence on concentration, and alkyl chain length of C_nTAB. The nano-dumbbells show plasmon-enhanced hydrogen evolution under visible and near-infrared light.

Photocatalysis has received significant attention for solar conversion to electricity or fuels based on electron-hole pair production in semiconductors.[1] However, this process is constrained mainly by low photocatalytic efficiency and limited visible and near-infrared (NIR) photoabsorption. Efficient engineering of the photocatalyst surface and interface is crucial to overcome these limitations.[2-5] Recently, surface plasmon resonance (SPR) of Au,[2,3,6-11] Ag[12-14] and Pd[15,16] nanoparticles has been applied to efficiently enhance visible and NIR absorption and generate SPR hot electrons.[4,17,18]

Among these nanostructures, AuNRs with tunable SPR are of particular interest due to the fact of their wide range of light harvesting; panchromatic absorption toward the solar spectrum can significantly improve the solar energy conversion efficiency.[11] Moreover, AuNRs are usually interfaced with efficient electron acceptors (such as semiconductor TiO_2,[19] graphene,[20] cocatalyst Pt[9]) to maximize the charge separation of hot electrons. Recently, we developed an autonomous, AuNR-TiO_2 based photocatalytic device with oxidation and reduction co-catalysts using nanofabrication techniques.[3] We clearly demonstrated that the plasmonic metal-semiconductor interface, which is a Schottky junction, can effectively select out the hot electrons; so that all charge carriers involved in the oxidation and reduction steps arise from these hot electrons, which are generated by the excitation of surface plasmons in the nanostructured AuNRs. In order to realize recycling of the photo-reduction/−oxidation, extraction of the hot electrons requires both refilling of these electrons and an electron donor accessible region on the SPR metal surface.[3,10,11,16,18,21-23] The spatial separation structure (rather than homogenous core-shell structure) can be provided by line-of-sight depositions using nanofabrication techniques that rely on advanced facilities and sophisticated operators. This nanofabrication method is usually not applicable for freestanding AuNRs synthesized by wet chemistry when there is no control of the orientation needed to create anisotropic AuNR-TiO_2 structures. Additionally, all wet-chemistry routes to such a well-defined spatial separation structure are challenging.

Anisotropic growth of TiO_2 onto AuNRs, instead of depositing AuNRs onto TiO_2,[24] could give better contact between Au and TiO_2. Because bilayers of surface-capping agents such as cetyltrimethylammonium bromide ($C_{16}TAB$) are more densely packed on AuNR sides than at the tips, this phenomenon has been utilized for the anisotropic overgrowth on $C_{16}TAB$-capped AuNRs with metal heterostructures or silica.[7,9,25] However, anisotropic overgrowth of semiconductors such as TiO_2 on $C_{16}TAB$-capped AuNRs in solution has been rarely reported.[26]

In this study, we report a wet-chemistry method for the anisotropic overgrowth of TiO_2 on AuNRs by using C_nTAB as a soft template and by controlling the degree of hydrolysis of $TiCl_3$. The roles of concentration and alkyl chain length of C_nTAB as well as the diameter of the AuNRs were carefully studied. The as-prepared TiO_2-tipped AuNRs have a dumbbell and spatial separation structure, and TiO_2 acts as a filter for hot electrons from AuNRs. This structure satisfies the electron refilling requirement and exhibits plasmon-enhanced hydrogen production from water reduction under visible and NIR light irradiation.

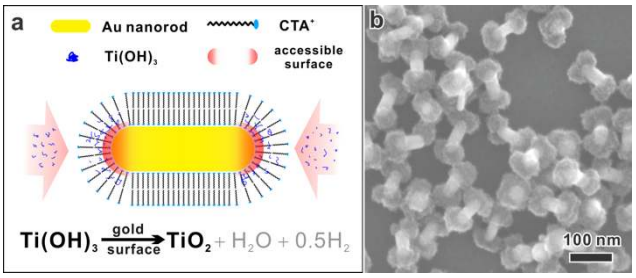

Figure 1. (a) Schematic showing the origin of anisotropic TiO_2 coating. (b) SEM image of the as-prepared AuNR-TiO_2 nanodumbbells. Synthetic condition: 32 nm AuNRs (in diameter), 13.9 mM $C_{16}TAB$.

Figure 1a illustrates the formation of the dumbbell nanoparticles by our bottom-up wet-chemistry method. The C_nTAB bilayer confines the AuNR with only the tips accessible to Ti species. By controlling the hydrolysis of $TiCl_3$ via the pH or the reaction solution with $NaHCO_3$,[27,28] Ti^{3+} is catalytically oxidized on the Au tips to form TiO_2. Figure 1b is a typical SEM image of as-prepared AuNR-TiO_2 nanodumbbells using C_{16}TAB-capped AuNRs as seeds (Figure S1). The product consists of uniform nanodumbbell structures with the two tips of all the AuNRs coated with TiO_2 caps and the sides exposed. During the coating process, red shifts of SPR bands are observed *in situ* in the UV-Vis spectra (Figure S2). This phenomenon corresponds to a local refractive index change due to the formation of the TiO_2 caps on the AuNR, and agrees with previous reports of dielectric material coatings on Au nanoparticles.[28-30] Due to the release of acid during the $TiCl_3$ hydrolysis, and the spatial coverage of the Au surface by the TiO_2 deposition, the reaction slows down after about 30 min. In the synthesis, the spatial selectivity of the TiO_2 deposition on the AuNRs is controlled by engineering their surface chemistry. Another type of nanoparticles, with a fully coated core-shell structure, can be prepared using a similar $TiCl_3$ hydrolysis process with the AuNRs pre-modified by an anionic surfactant, sodium dodecyl sulfate (SDS, Figure S3).

The anisotropic overgrowth of TiO_2 on AuNRs is further shown by TEM and HAADF-STEM-EDX analyses (Figure 2 and Figure S4). The micrograph reveals that the TiO_2 caps are porous with basic building blocks smaller than 2 nm. The elemental mapping of the as-prepared product confirms that the two caps are made from TiO_2. The signal distribution obtained by linear scanning in the longitude direction clearly indicates the existence of two symmetrical TiO_2 caps. No Ti signal has been found by transverse scanning through the lateral side, further confirming specific tip-side selectivity of the deposition. Furthermore, the significant distribution difference and shape of the caps suggest that the anisotropic deposition of TiO_2 is initiated from two tips of each AuNR and then extended towards the middle side surface of AuNRs. Note that the TiO_2 caps are amorphous based on the TiO_2 ultrafine domain size revealed in the HRTEM and XRD patterns (Figure S5).

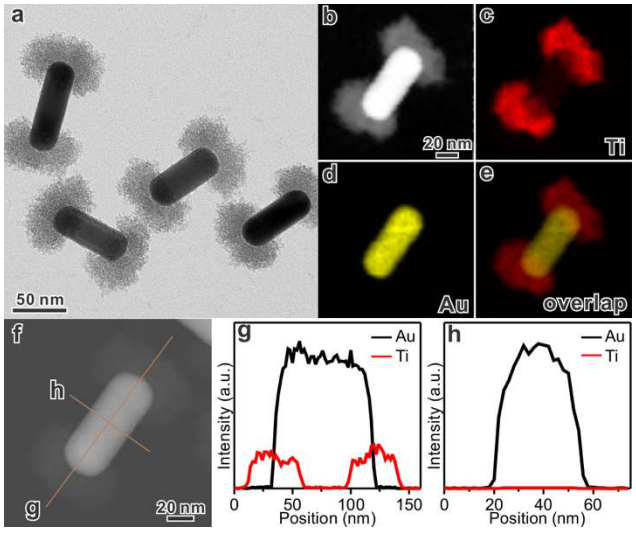

Figure 2. (a) TEM image, (b-e) HAADF-STEM image and elemental maps and (f-h) Au and Ti elemental profiles of AuNR-TiO_2 nanodumbbells.

Anisotropic overgrowth of TiO_2 on the AuNR tips can be explained by the bilayer adsorption structure of C_{16}TAB and the special structure of the AuNR tips. The bilayer can behave as a soft template that guides the preferential bonding of the Au surface to solution species. Due to the curvature difference, the assembly of C_{16}TAB on both tips of AuNR is less compact than that on the side.[25,31] The lower obstruction in these regions allows solution species to approach the AuNR tip surface (Figure 1a). This phenomenon has been previously used for the selective surface functionalization of AuNR tips.[32-34] By generalizing the side/tip selective functionalization for hydrolysis reactions, Wang's group successfully prepared AuNRs with an anisotropic SiO_2 or Ag_2O coating.[25,35] Similarly, here the TiO_2 formation process (which is a hydrogen evolution reaction due to the oxidation of the $TiCl_3$ precursor[27]) can be selectively catalyzed by the accessible AuNR tips, resulting in the spatially selective coating of TiO_2 on AuNRs. The anisotropic overgrowth can be due to both less dense assembly of C_{16}TAB and herein less electrostatic repulsion between Ti species and the positively-charged C_{16}TAB bilayer.[34,36,37] In contrast, SDS or similar surfactants modified AuNRs have a more random molecular assembly on them, resulting in homogenous overgrowth of TiO_2 on AuNRs.[28,34]

In order to gain a deeper understanding of why C_{16}TAB promoted the anisotropic growth of TiO_2, the relation between the growth and the concentration of C_{16}TAB was studied. Figure 3 and Figure S6 show the C_{16}TAB concentration effect on TiO_2 growth using the same AuNRs of 32nm in diameter. In order to reach a >90% yield of AuNR-dumbbells, the C_{16}TAB concentration must be appropriate, that is, in the range between its first critical micelle concentration (1st CMC, 0.89 mM[38]) and its 2nd CMC (20 mM[38]). When C_{16}TAB concentration is lower than the 1st CMC, most of the AuNRs are fully covered with a rough TiO_2 shell, due to the unstable and easily disrupted C_{16}TAB bilayer.[34] When the C_{16}TAB concentration is greater than the 2nd CMC, a large portion of the product has only one tip coated with TiO_2, or is not coated at all, due to the ultra-dense bilayer of C_{16}TAB. However, for concentrations of C_{16}TAB between the 1st and 2nd CMC, the deposition of TiO_2 is effectively limited to two tips with a high yield. A similar result was reported by Wang et al,[25] i.e., an appropriate C_{16}TAB concentration (~6 mM) leads to effective overgrowth of SiO_2 onto AuNR tips. These results show that a well-assembled C_{16}TAB bilayer is critical for the anisotropic overgrowth of TiO_2 on AuNRs.

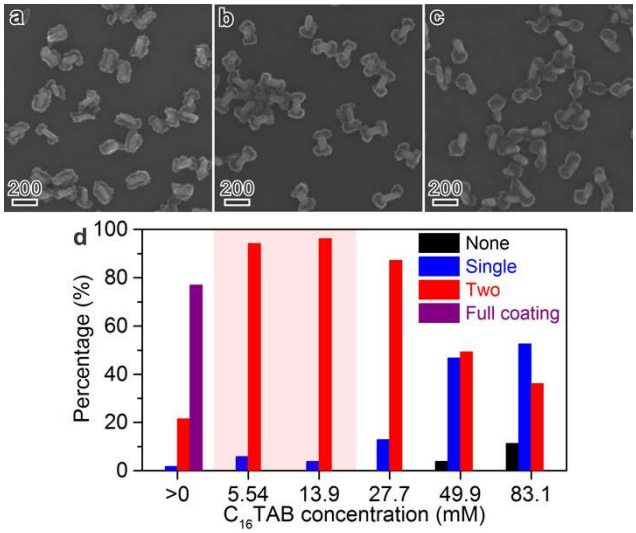

Figure 3. C_{16}TAB concentration effect in TiO_2 growth on AuNRs. The same AuNR diameter (32 nm), but different C_{16}TAB concentrations: (a) no additional C_{16}TAB, (b) 5.54 mM, and (c) 83.1 mM. (d) The percentage histogram of coated AuNR tips. Note that the pink shadow indicates the C_{16}TAB concentration between its 1st and 2nd CMC.

Based on the assumption of the relationship between the selective coating and the C_{16}TAB bilayer, curvatures of the AuNR tips should play a critical role. AuNRs with different diameters as the seeds were used in the presence of the same C_{16}TAB concentration. The histogram in Figure 4a shows a correlation of AuNR diameters and the percentage of coated tips in the products. The trend shows that the thinner AuNRs, the harder it is to coat TiO_2 on the tips of the AuNRs (regardless of their lengths). A large percentage of the products formed using narrow AuNRs (diameter smaller than 20 nm) are either coated on a single tip or are completely without coating (Figure S7). Since the curvature has a reciprocal relationship with the diameter, seemingly the C_{16}TAB bilayer on thinner AuNRs should have a more open structure on the tips, which should allow the region to be coated more easily. On the other hand, the area on the tip of a thinner AuNR is also significantly reduced. The decreased tip area may dramatically reduce the ability of nucleating TiO_2 caps. For example, considering the hemisphere area on the tips of AuNRs and assuming the same TiO_2 coating length (10-20 nm, based on TEM analysis) from the tips along the NRs, the coated surface area will be reduced by 20-30% when the AuNR diameter is reduced from 32 to 27 nm; this obviously changes the ability to form the TiO_2 caps on AuNRs and their stability. As shown in Figure 4a, the onset diameter of this change is about 20 nm. In addition, Au does not have strong chemical binding to amorphous TiO_2. From our observations, the overall effect of reducing the AuNR diameter is dominated by this stability aspect.

Since C_{16}TAB cannot lead to the coating of thin AuNRs (<27 nm in diameter) to give a high yield of TiO_2 overgrowth, other C_nTABs with shorter alkyl chain were studied. Figure 4b and Figure S8 shows the result of coating TiO_2 onto thin AuNRs (22 nm in diameter) in the presence of single C_nTAB (x=12, 14, 16; note that the same molar concentration optimized for C_{16}TAB were used thoroughly). The yield of tip-selective coating on thin AuNRs is significantly improved when using C_{14}TAB or C_{12}TAB instead of C_{16}TAB. Their shorter hydrocarbon chains give a weaker hydrophobic interaction between molecules, so that better permit a bilayer adsorption structure on the thin AuNR tip surface. Especially on the tips of thin AuNRs, the C_{14}TAB or C_{12}TAB bilayer allows Ti(III) species access to the catalytic Au surface more easily in spite of the higher curvature, therefore makes a thicker TiO_2 deposition possible and thus compensates the instability from the smaller area on the tips of thin AuNRs. Furthermore, AuNR diameter effect in the presence of C_{12}TAB (13.9 mM; its 1st CMC is ~14 mM[39]) was studied (Figure S9). For 15 nm AuNRs, C_{12}TAB leads to higher possibility of tipped TiO_2 coating than C_{16}TAB, which is converse for the case of 32 nm AuNRs. Indeed, our studies reveal that an optimum combination of C_nTAB with specific carbon chain length and AuNR diameter is essential in order to obtain a high-yield anisotropic overgrowth of TiO_2 onto AuNR tips. Previous investigations were conducted using C_{18}TAB or C_{18}TAC for the overgrowth of metal heterostructures or silica on AuNRs with limited diameters[7,9,25]; here we focus on varying the C number in C_nTAB to control the capping agent functionality in heterogeneous overgrowth processes of TiO_2 on AuNRs with various diameters.

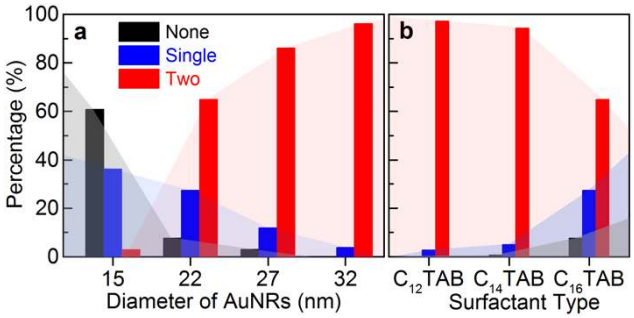

Figure 4. Percentage histogram of coated tips on AuNR-TiO_2 product synthesized under similar conditions, with (a) the same concentration of C_{16}TAB (13.9 mM), but different AuNR diameters, and (b) same AuNR diameter (22 nm), but different C_nTABs (13.9 mM).

It should be noted that mixing two C_nTABs with different chain lengths (values of n) can change the growth behavior of TiO_2 on AuNRs when compared to growth using a single C_nTAB. Figure S10 shows the product prepared in a mixed C_{12}TAB/C_{16}TAB (1:1) solution. In this case, TiO_2 is inclined to coat the sharp corners which connect the side and the endmost tips of AuNRs, rather than the whole tips as in the case of single C_nTAB (Figure S7d, S9d). This is also attributed to the limitation from C_nTAB bilayer structure. As a mixture of two C_nTABs, the entropic force makes C_{16}TAB with longer hydrocarbon chains (C_{16}) go to the less curved surface and push the shorter C_{12}TAB aside to corners. The higher percentage of shorter C_{12}TAB on sharp corners significantly reduces the hindrance for TiO_2 deposition on that focused region and allows it to form small caps on the AuNR tips.

The most exciting feature of the designed AuNR-TiO_2 nanodumbbells is their ability to promote SPR-induced hot-electron

generation under visible and NIR light. While AuNR@TiO_2 core-shell nanoparticles and pure amorphous TiO_2 show no activity for hydrogen evolution, AuNR-TiO_2 nanodumbbells exhibit relatively high photoactivity, compared to physically mixed AuNRs and amorphous TiO_2 (Figure 5a; AuNR#5 with 32-nm diameter were used). Note that the difference in the photocatalytic activity of these three samples does not result from the surface area or the mass of TiO_2, since amorphous TiO_2 itself does not absorb visible light and a significantly excess quantity of TiO_2 was used in the mechanical mixture of AuNRs and TiO_2. The activity of AuNR-TiO_2 nanodumbbells is higher than that of spherical Au nanoparticles deposited on crystalline TiO_2 under similar condition.[40] Further increasing the crystallinity of the TiO_2 and adding co-catalysts could enhance the visible light performance of our AuNR-TiO_2 dumbbells.[3] These control experiments clearly demonstrate the importance of AuNR-dumbbell structure with intimate physical contact and strong plasmonic coupling for enhanced charge separation in the plasmon-enhanced photocatalysis. The difference of the photocatalytic activities under visible light for the AuNR-TiO_2 nanodumbbells and the AuNR@TiO_2 core-shell structure further suggests that the plasmon-enhanced photocatalysis mechanism is plasmonic hot electron transfer due to localized surface plasmon resonance of AuNRs (which is dependent on the configuration/architecture of metal-semiconductor heterojunction), rather than plasmon-induced resonance energy transfer (based on the inactivity of the core-shell structure).[41,42]

Hot electron generation was further demonstrated in the photoreduction of methylene blue (MB), a model acceptor molecule (Figure 5b). After 60 min of irradiation, the AuNR-TiO_2 dumbbells exhibited reduction of ~60% of the MB dye. In the control experiments, physically mixed AuNRs and TiO_2 solution exhibited reduction of ~10% of the MB, while AuNR@TiO_2 core-shell structure showed insignificant activity (<1%; moreover, part of the activity may come from photobleaching[43]). These experiments on the photoreduction of MB demonstrate the importance of close contact and the anisotropic assembly of the AuNR and TiO_2 domains for effective visible light photocatalysis.

Previous studies indicate that the SPR-induced hot electrons can be filtered out from metal nanoparticles with the positive charges left behind.[3,4,11,18,34] Note that neither TiO_2 alone nor pure AuNRs can produce hydrogen under similar conditions. For the nanodumbbells, the oxidation pathway is on their side surface (Figure 5c), where the lateral side of AuNRs can be directly exposed to electron donors so that oxidation reactions can take place. With AuNR partially exposed in the dumbbell structure, AuNRs generate a concentrated electromagnetic field that focuses energy flux around the semiconductor, and thus enhance hot-electron generation and photocatalytic activity.[3,9,18,44,45] As pointed out by Yates,[46] metal-TiO_2 contact induces band bending in TiO_2 which can be used either for electron or hole transfer, depending on whether that band bends upward or downward, which, in turn, depends on the relative ordering of the semiconductor's and metal's Fermi levels. The Femi level of TiO_2 is higher than that of Au, causing the bands of the TiO_2 to bend upward at the interface between these two materials (at which a Schottky junction is formed). At the interface, electrons would flow "down" and holes "up" in the bent conduction band and valence band respectively, as shown in energy band diagrams.[46] Holes generated in AuNRs under visible light are, therefore, unlikely to transfer to TiO_2. In contrast, hot electrons generated in AuNRs under visible light that overcome the Schottky barrier are likely to flow from AuNRs to TiO_2 and be available for photo-reduction with TiO_2 acting as the electron transfer medium. The dumbbell structure ideally exploits such charge exchange opportunities, carrying out reduction processes on the TiO_2 then restoring charge balance to the Au core through oxidation reactions that would occur on the bare portions of the AuNRs (Figure 5c). A fully coated AuNR is denied of the opportunity for establishing such a complete circuit that allows both electrons and holes to access their appropriate reaction partners, thereby blocking the continuous flow of the hot charge carriers resulting from the excitation of the SPR (Figure 5d). We, therefore, ascribe the better SPR photocatalytic performance of the dumbbells to their ability to present appropriate and separate regions at which the oxidation and reduction processes can take place, as opposed to the core-shell nanoparticles without such separate regions.

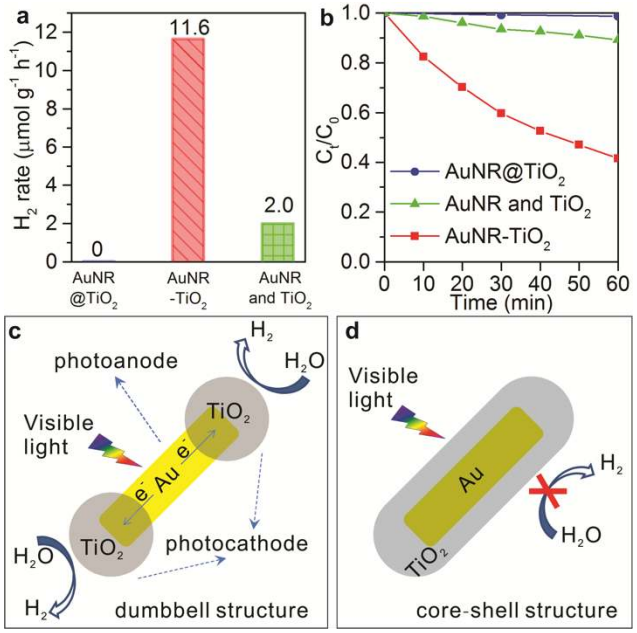

Figure 5. Comparison of (a) hydrogen evolution rate by various catalysts, and (b) normalized concentration of MB dye vs irradiation time; both under visible illumination and in the presence of methanol and water. (c-d) Structure and mechanism of operation under visible light of (c) an individual AuNR-TiO_2 dumbbell and (d) core-shell AuNR@TiO_2. In (c), hot electrons generated from plasmonic AuNRs are filtered out by the Au-TiO_2 Schottky barrier for photo-reduction and regenerated from the electron donor (methanol here).

In summary, an easy, bottom-up, wet-chemistry technique for the synthesis of anisotropic TiO_2 overgrowth on AuNRs has been developed using the selective spatial assembly of a C_nTAB bilayer on AuNR surfaces and the hydrolysis of $TiCl_3$. The concentration, alkyl chain length of C_nTAB, and the diameter of AuNRs are important in order to control the selective overgrowth. The as-prepared AuNR-TiO_2 nanodumbbells exhibit plasmon-enhanced hydrogen evolution under visible-NIR light. The created AuNR-TiO_2 interface with the AuNR side exposed, as a Schottky junction, can filter out SPR hot electrons from the AuNRs. Engineering the structure, such as loading co-catalysts, may further improve its activity for the plasmon-induced hydrogen evolution.

This work shows an alternative solution of anisotropic TiO_2 overgrowth rather than nanofabrication techniques, and is expected to be a promising platform for the development of free-standing functional photocatalysts.

ASSOCIATED CONTENT

Supporting Information

Experimental details, TEM, HRTEM, SEM images, XRD, UV-vis spectra. This material is available free of charge via the Internet at http://pubs.acs.org.

AUTHOR INFORMATION

Corresponding Author

*E-mail: stucky@chem.ucsb.edu

Author Contributions

§These authors contributed equally.

Present Addresses

#Department of chemical and biochemical engineering, University of Iowa, Iowa City, IA 52242, USA

Notes

The authors declare no competing financial interests.

ACKNOWLEDGMENT

This research was supported by the Center for Energy Efficient Materials, an Energy Frontier Research Center funded by the U.S. Department of Energy, Office of Science, Basic Energy Sciences under award no. DE-SC0001009 and by the National Science Foundation (DMR 0805148). The MRL Shared Experimental Facilities are supported by the MRSEC Program of the NSF under award no. DMR 1121053; a member of the NSF-funded Materials Research Facilities Network(www.mrfn. org). B.W. was partially supported by China Scholarships Council for this research. We gratefully acknowledge Jialuo Li (TAMU) for help with drawing the schematic TOC figure.

REFERENCES

(1) Ma, Y.; Wang, X. L.; Jia, Y. S.; Chen, X. B.; Han, H. X.; Li, C. *Chem. Rev.* **2014**, *114*, 9987.

(2) Tada, H.; Mitsui, T.; Kiyonaga, T.; Akita, T.; Tanaka, K. *Nat. Mater.* **2006**, *5*, 782.

(3) Mubeen, S.; Lee, J.; Singh, N.; Kramer, S.; Stucky, G. D.; Moskovits, M. *Nat. Nanotechnol.* **2013**, *8*, 247.

(4) Kochuveedu, S. T.; Jang, Y. H.; Kim, D. H. *Chem. Soc. Rev.* **2013**, *42*, 8467.

(5) Liu, C.; Tang, J. Y.; Chen, H. M.; Liu, B.; Yang, P. D. *Nano Lett.* **2013**, *13*, 2989.

(6) Tian, Y.; Tatsuma, T. *J. Am. Chem. Soc.* **2005**, *127*, 7632.

(7) Wang, F.; Li, C. H.; Chen, H. J.; Jiang, R. B.; Sun, L. D.; Li, Q.; Wang, J. F.; Yu, J. C.; Yan, C. H. *J. Am. Chem. Soc.* **2013**, *135*, 5588.

(8) Wu, K. F.; Rodriguez-Cordoba, W. E.; Yang, Y.; Lian, T. Q. *Nano Lett.* **2013**, *13*, 5255.

(9) Zheng, Z. K.; Tachikawa, T.; Majima, T. *J. Am. Chem. Soc.* **2014**, *136*, 6870.

(10) Moskovits, M. *Nat. Nanotechnol.* **2015**, *10*, 6.

(11) Mubeen, S.; Lee, J.; Liu, D. Y.; Stucky, G. D.; Moskovits, M. *Nano Lett.* **2015**, *15*, 2132.

(12) Christopher, P.; Xin, H. L.; Linic, S. *Nat. Chem.* **2011**, *3*, 467.

(13) Li, G.; Cherqui, C.; Bigelow, N. W.; Duscher, G.; Straney, P. J.; Millstone, J. E.; Masiello, D. J.; Camden, J. P. *Nano Lett.* **2015**, *15*, 3465.

(14) Ingram, D. B.; Linic, S. *J. Am. Chem. Soc.* **2011**, *133*, 5202.

(15) Long, R.; Mao, K. K.; Gong, M.; Zhou, S.; Hu, J. H.; Zhi, M.; You, Y.; Bai, S.; Jiang, J.; Zhang, Q.; Wu, X. J.; Xiong, Y. J. *Angew. Chem. Int. Ed.* **2014**, *53*, 3205.

(16) Long, R.; Rao, Z.; Mao, K.; Li, Y.; Zhang, C.; Liu, Q.; Wang, C.; Li, Z. Y.; Wu, X.; Xiong, Y. *Angew. Chem. Int. Ed.* **2015**, *54*, 2425.

(17) Jiang, R.; Li, B.; Fang, C.; Wang, J. *Adv. Mater.* **2014**, *26*, 5274.

(18) Clavero, C. *Nat Photon* **2014**, *8*, 95.

(19) Pu, Y. C.; Wang, G. M.; Chang, K. D.; Ling, Y. C.; Lin, Y. K.; Fitzmorris, B. C.; Liu, C. M.; Lu, X. H.; Tong, Y. X.; Zhang, J. Z.; Hsu, Y. J.; Li, Y. *Nano Lett.* **2013**, *13*, 3817.

(20) Hoggard, A.; Wang, L. Y.; Ma, L. L.; Fang, Y.; You, G.; Olson, J.; Liu, Z.; Chang, W. S.; Ajayan, P. M.; Link, S. *ACS Nano* **2013**, *7*, 11209.

(21) Furube, A.; Du, L.; Hara, K.; Katoh, R.; Tachiya, M. *J. Am. Chem. Soc.* **2007**, *129*, 14852.

(22) Wang, C.; Astruc, D. *Chem. Soc. Rev.* **2014**, *43*, 7188.

(23) DuChene, J. S.; Sweeny, B. C.; Johnston-Peck, A. C.; Su, D.; Stach, E. A.; Wei, W. D. *Angew. Chem. Int. Ed.* **2014**, *53*, 7887.

(24) Liu, L. Q.; Ouyang, S. X.; Ye, J. H. *Angew. Chem. Int. Ed.* **2013**, *52*, 6689.

(25) Wang, F.; Cheng, S.; Bao, Z.; Wang, J. *Angew. Chem. Int. Ed.* **2013**, *52*, 10344.

(26) Seh, Z. W.; Liu, S. H.; Zhang, S. Y.; Bharathi, M. S.; Ramanarayan, H.; Low, M.; Shah, K. W.; Zhang, Y. W.; Han, M. Y. *Angew. Chem. Int. Ed.* **2011**, *50*, 10140.

(27) Liu, R.; Sen, A. *J. Am. Chem. Soc.* **2012**, *134*, 17505.

(28) Fang, C. H.; Jia, H. L.; Chang, S.; Ruan, Q. F.; Wang, P.; Chen, T.; Wang, J. F. *Energ. Environ. Sci.* **2014**, *7*, 3431.

(29) Chen, H. J.; Wang, F.; Li, K.; Woo, K. C.; Wang, J. F.; Li, Q.; Sun, L. D.; Zhang, X. X.; Lin, H. Q.; Yan, C. H. *ACS Nano* **2012**, *6*, 7162.

(30) Li, B. X.; Gu, T.; Ming, T.; Wang, J. X.; Wang, P.; Wang, J. F.; Yu, J. C. *ACS Nano* **2014**, *8*, 8152.

(31) Zhang, S. Z.; Kou, X. S.; Yang, Z.; Shi, Q. H.; Stucky, G. D.; Sun, L. D.; Wang, J. F.; Yan, C. H. *Chem. Commun.* **2007**, 1816.

(32) Nie, Z. H.; Fava, D.; Kumacheva, E.; Zou, S.; Walker, G. C.; Rubinstein, M. *Nat. Mater.* **2007**, *6*, 609.

(33) Liu, K.; Zhao, N. N.; Kumacheva, E. *Chem. Soc. Rev.* **2011**, *40*, 656.

(34) Chen, H.; Shao, L.; Li, Q.; Wang, J. *Chem. Soc. Rev.* **2013**, *42*, 2679.

(35) Bao, Z. H.; Sun, Z. H.; Xiao, M. D.; Chen, H. J.; Tian, L. W.; Wang, J. F. *J. Mater. Chem.* **2011**, *21*, 11537.

(36) Perez-Juste, J.; Liz-Marzan, L. M.; Carnie, S.; Chan, D. Y. C.; Mulvaney, P. *Adv. Funct. Mater.* **2004**, *14*, 571.

(37) Correa-Duarte, M. A.; Pérez-Juste, J.; Sánchez-Iglesias, A.; Giersig, M.; Liz-Marzán, L. M. *Angew. Chem. Int. Ed.* **2005**, *44*, 4375.

(38) Li, N. B.; Liu, S. P.; Luo, H. Q. *Anal. Lett.* **2002**, *35*, 1229.

(39) Bahri, M. A.; Hoebeke, M.; Grammenos, A.; Delanaye, L.; Vandewalle, N.; Seret, A. *Colloid Surface A* **2006**, *290*, 206.

(40) Ding, D.; Liu, K.; He, S.; Gao, C.; Yin, Y. *Nano Lett.* **2014**, *14*, 6731.

(41) Cushing, S. K.; Bristow, A. D.; Wu, N. *Phys. Chem. Chem. Phys.* **2015**, *17*, 30013.

(42) Cushing, S. K.; Li, J. T.; Bright, J.; Yost, B. T.; Zheng, P.; Bristow, A. D.; Wu, N. Q. *J. Phys. Chem. C* **2015**, *119*, 16239.

(43) Costi, R.; Saunders, A. E.; Elmalem, E.; Salant, A.; Banin, U. *Nano Lett.* **2008**, *8*, 637.

(44) Cushing, S. K.; Li, J.; Meng, F.; Senty, T. R.; Suri, S.; Zhi, M.; Li, M.; Bristow, A. D.; Wu, N. *J. Am. Chem. Soc.* **2012**, *134*, 15033.

(45) Hou, W. B.; Hung, W. H.; Pavaskar, P.; Goeppert, A.; Aykol, M.; Cronin, S. B. *ACS Catal.* **2011**, *1*, 929.

(46) Zhang, Z.; Yates, J. T. *Chem. Rev.* **2012**, *112*, 5520.